Stability of periodic arrays of vortices

Thierry Dauxois,[a] Stephan Fauve, and Laurette Tuckerman[b]
Laboratoire de Physique, URA-CNRS No. 1325, Ecole Normale Supérieure de Lyon, 46 Allée d'Italie, 69364 Lyon Cedex 07, France

(Received 14 June 1995; accepted 11 October 1995)

The stability of periodic arrays of Mallier–Maslowe or Kelvin–Stuart vortices is discussed. We derive with the energy-Casimir stability method the nonlinear stability of this solution in the inviscid case as a function of the solution parameters and of the domain size. We exhibit the maximum size of the domain for which the vortex street is stable. By adapting a numerical time-stepping code, we calculate the linear stability of the Mallier–Maslowe solution in the presence of viscosity and compensating forcing. Finally, the results are discussed and compared to a recent experiment in fluids performed by Tabeling *et al.* [Europhy. Lett. **3**, 459 (1987)]. Electromagnetically driven counter-rotating vortices are unstable above a critical electric current, and give way to co-rotating vortices. The importance of the friction at the bottom of the experimental apparatus is also discussed. © *1996 American Institute of Physics.* [S1070-6631(96)00102-5]

I. INTRODUCTION

The problem of vortex dynamics is important for the field of chaotic motion and dynamical systems theory, but the discovery of coherent structures in turbulence has fostered the hope that the study of vortices will also lead to a better understanding of turbulent flows.[1] The emergence of coherent flow structures is a well-known feature of quasi-geostrophic flows,[2] soap films or two-dimensional turbulence[3] and, because of their relevance to large-scale geophysical flows, the dynamics of these structures has attracted attention during the past two decades. Geophysical fluid flows often appear to be dominated by a strong but localized vortical structure that lasts for many circulation times even when relatively turbulent flows are impinging upon it. Experimental evidence indicates also that the planar free shear layer has an organized two-dimensional structure over a wide range of Reynolds numbers.[4,5] When modelling steady-state configurations of geophysical flows as solutions of a dynamical system, it is important to analyze their stability in order to see if they can describe physically observable situations. Indeed, in the real world, many random forces act on the system and the stationary situations we observe must be stable under these perturbations.

The dynamics of coherent structures in two-dimensional geometry has been studied in many different experiments using rotating or stratified fluid (see Ref. 6 and references therein), in a shallow layer of mercury[7] or of electrolyte[8] subjected to a magnetic field. Here let us recall the experiment proposed by Tabeling *et al.*[9] A periodic array of counter-rotating vortices is driven by electromagnetic forcing. By passing a current through a cell containing a solution of sulfuric acid and an array of permanent magnets of alternating polarity at the bottom of the cell, the Lorentz force stirs the fluid, producing the vortices. The two-dimensionality of the flow is ensured using a shallow fluid layer. The basic results can be summarized as follows:

(i) At low current corresponding to weak forcing and hence low Reynolds number, the flow consists of a linear array of counter-rotating vortices.

(ii) This state becomes unstable beyond a critical current. The linear array is now composed of nonuniform tilted vortices, alternately large and small.

(iii) A further increase in the current leads to a state with half the number of co-rotating vortices as compared to the initial state.

This experiment has led to a number of studies concerning chaotic regimes.[10] Let us present another point of view. The first question we want to address is the following: what is the connection between the patterns of the Navier–Stokes equation and the exact solutions of the Euler equation, where solutions of this type are known to exist? The second question is to determine the stability of such coherent structures in the presence of viscosity and forcing.

We have organized the article in the following way. In Sec. II, we review some steady-state solutions of the two-dimensional inviscid and incompressible fluid motion. We will also present the Mallier–Maslowe vortex street that we will study in the remainder of the article. Sections III, IV and V form the heart of the paper. In Sec. III, we derive analytically explicit sufficient conditions for the nonlinear stability estimates in the inviscid case, using Casimirs and convexity properties. In Sec. IV, we discuss the two-dimensional viscous flows and present the numerical method used for studying the linear stability. Section IV C discusses the results. Section IV D sets up the correspondence between the results and the experiment. Finally, in Sec. V, the nonlinear evolution of an unstable Mallier–Maslowe solution is presented. The results are then discussed in connection with the experiments of Tabeling *et al.*[9]

II. INVISCID FLOW

For two-dimensional incompressible fluid motion, one obtains from the Navier–Stokes equation, by elimination of the pressure, the equation for the stream function ψ:

[a]tdauxois@physique.ens-lyon.fr
[b]Permanent address: LIMSI, BP 133, 91403 Orsay Cedex, France.

$$\frac{\partial \nabla^2 \psi}{\partial t} + J(\nabla^2 \psi, \psi) = \nu \nabla^4 \psi + G_{ext} \tag{1}$$

where $J(A,B) = A_x B_y - A_y B_x$ is the usual Poisson bracket and ν the kinematic viscosity. The last term G_{ext} is due to possible external forcing.

In the absence of external forcing and viscosity, the vorticity equation reduces to the Euler equation:

$$\frac{\partial \nabla^2 \psi}{\partial t} = J(\psi, \nabla^2 \psi). \tag{2}$$

For steady-state flows, this gives

$$J(\psi, \nabla^2 \psi) = 0. \tag{3}$$

Hence it follows that the vorticity $\omega = -\nabla^2 \psi$ is constant along contours of constant stream function ψ. The study of planar steady-state flows in an ideal incompressible liquid is consequently reduced to solving the following equation:

$$\nabla^2 \psi = \frac{\partial^2 \psi}{\partial x^2} + \frac{\partial^2 \psi}{\partial y^2} = F(\psi) \tag{4}$$

where F is an arbitrary function. This is a nonlinear elliptic equation for ψ and therefore admits a continuous multiplicity of solutions associated with the arbitrariness of $F(\psi)$. The problem of finding steady states of two-dimensional vortices in an inviscid fluid is then equivalent to solving the Poisson equation for the electrostatic potential with the charge density self-consistently determined.

The simplest choice for F is a linear function, which already gives many different patterns. Indeed Kolmogorov flows, cellular structures with square or hexagonal cells and even quasi-crystal patterns are solutions[11] of the Helmholtz equation $\nabla^2 \psi = -\psi$. Many other solutions have been studied in the literature such as the Lamb dipole[12,13] and the nonsymmetric Chaplygin dipolar solutions.[14]

A possible choice for the function F which has been proposed in the literature[15–17] is

$$\frac{\partial^2 \psi}{\partial x^2} + \frac{\partial^2 \psi}{\partial y^2} = -\frac{(1-\varepsilon^2)}{2} \sinh(2\psi). \tag{5}$$

This $\omega - \psi$ sinh-relationship is very important because, using a statistical approach, one can show[18] that it characterizes the most probable state of a two-dimensional system of ideal point vortices. Published data showing the functional dependence of vorticity on stream function in long-lived structures, seen in experiments and simulations, seem qualitatively consistent with hyperbolic-sine [as in Eq. (5)] or exponential profiles [as in Eq. (7) below] which follow from entropy maximization.[19] These studies have been verified by very long-time high resolution numerical studies; however, recent work shows some evidence that this result depends on the initial conditions.[13] Another recent experimental study[20] led to the conclusion that the maximum entropy state is unlikely to be reached since the observed final states of flow display characteristics that conflict with the statistical theory.

In the case of an infinite box, the solution to Eq. (5) introduced by Mallier and Maslowe[21] which we will discuss in the remainder of the article is:

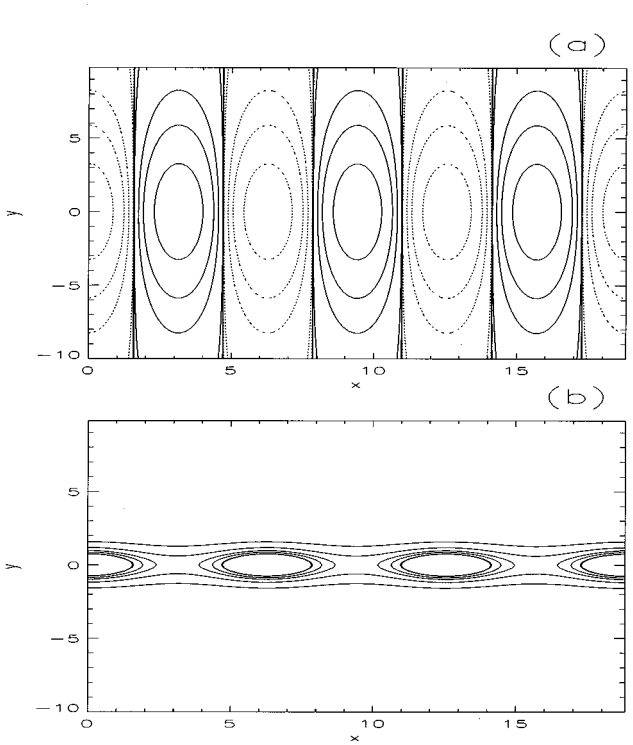

FIG. 1. Steady Flows. (a) represents the streamlines of the Mallier–Maslowe solution (6) for $\varepsilon = 0.3$. (b) represents the streamlines of the Kelvin–Stuart solution (7) for $\varepsilon = 0.3$. The dashed curves are negative contour lines and the solid curves are positive ones.

$$\psi_M = \ln\left(\frac{\cosh \varepsilon y - \varepsilon \cos x}{\cosh \varepsilon y + \varepsilon \cos x}\right) = -2 \operatorname{arctanh}\left(\frac{\varepsilon \cos x}{\cosh \varepsilon y}\right) \tag{6}$$

which describes a stationary pattern in the form of a street of counter-rotating vortices, arranged periodically along the x-axis at intervals of π. A typical solution is shown in Fig. 1(a) for $\varepsilon = 0.3$. The parameter ε characterizes the vorticity density: when $\varepsilon = \pm 1$, we recover the point vortex solution and when $\varepsilon = 0$ we have $\psi = 0$. Thus, as ε ranges from 0 to 1, the flow represented by Eq. (6) ranges from the fluid at rest, to the flow due to a set of point vortices on the x-axis.

A third choice for the function F of Eq. (4) is that of J. T. Stuart,[22] an exponential function:

$$\frac{\partial^2 \psi}{\partial x^2} + \frac{\partial^2 \psi}{\partial y^2} = (1-\varepsilon^2) e^{-2\psi}. \tag{7}$$

If we use the change of variable proposed above, this equation is directly related to the well-known Liouville equation for a real scalar field $\psi(y,t)$, studied by both Liouville[23] and by Poincaré.[24]

The exact nonlinear solution to Eq. (7):

$$\psi_S = \ln(\cosh y + \varepsilon \cos x). \tag{8}$$

is called Kelvin–Stuart's cat's eyes[22] and is illustrated in Fig. 1(b). This solution can be derived in an elegant way with the Hirota method, assuming a vortex spacing of 2π. This solution is of interest because the solution corresponds qualitatively to the co-rotating vortices seen by Tabeling *et al.*[9]

Analytical expressions of the co-rotating or counter-rotating vortex streets are especially useful for studying the stability of the experimental fluid flows[9] described before. It would be of interest to find an analytic function connecting the co-rotating and counter-rotating solutions. As written by Mallier and Maslowe,[21] if such a function exists, it is likely that at the best the general equation will be the following:

$$\frac{\partial^2\psi}{\partial x^2}+\frac{\partial^2\psi}{\partial y^2}=Ae^{2\psi}+Be^{-2\psi}. \tag{9}$$

It can be shown that, rather than interpolating between Eq. (5) and Eq. (7), Eq. (9) reduces to the sinh-Poisson equation (5) for all nonzero values of A. Therefore a solution of Eq. (9) is

$$\psi=\ln\left(\frac{\cosh\ \varepsilon y-\varepsilon\ \cos\ x}{\cosh\ \varepsilon y+\varepsilon\ \cos\ x}\right)-\psi_0, \tag{10}$$

where $\varepsilon=(1-4\sqrt{-AB})^{-1/2}$ and $\psi_0=1/2\ \text{arccosh}[(B-A)/2(-AB)^{1/2}]$.

Moreover, it is possible to treat the Liouville equation (7) corresponding to the limiting case $A=0$, as a singular limit of the sinh-Poisson equation[25] by making the substitution $1-\varepsilon^2=\lambda^2e^{-2\beta}$ and $\psi=u-\beta$ in Eq. (5), and then taking $\beta\to+\infty$. By carefully following what happens in this highly singular limit, Tracy *et al.*[26] succeeded in exhibiting the Liouville solution as a singular limit of the sinh-Poisson solution. However, to our knowledge, the function connecting the two solutions has not been found. At this point, let us turn our attention to determining the nonlinear stability of the Mallier–Maslowe solutions.

III. NONLINEAR STABILITY OF THE COUNTER-ROTATING VORTICES

We are interested in the stability of the Mallier–Maslowe solution (6) in order to explain the experimental results presented by Tabeling *et al.*[9] To establish explicit sufficient stability conditions[27] for all values of ε and to study the nonlinear stability of the counter-rotating vortices in a domain D of the plane R^2, in the former article,[28] we used the total energy on this domain

$$\begin{aligned}H(\omega)&=\int\int_D\frac{1}{2}|\mathbf{v}|^2dx\ dy\\&=\int_{\partial D}\frac{1}{2}\psi\boldsymbol{\nabla}\psi.\mathbf{n}ds-\int\int_D\frac{1}{2}\psi\nabla^2\psi dx\ dy\\&=\frac{1}{2}\int\int_D\psi\omega dx\ dy\end{aligned} \tag{11}$$

where we have used the fact that the velocity, and hence $\boldsymbol{\nabla}\psi$, vanishes on the boundary of D. Since the fluid is inviscid, this quantity is conserved. More generally, one can also show,[29] that the functionals $C_\Phi(\omega)=\int\int_D\Phi(\omega)dx\ dy$, called Casimirs, are also conserved for any real-valued function Φ.

We define a conserved quantity $H_\Phi\equiv H+C_\Phi$ whose functional derivative is:

$$DH_\Phi(\omega).\delta\omega=\int\int_D(\psi(\omega)+\Phi'(\omega))\delta\omega dx\ dy. \tag{12}$$

We wish to choose Φ so that $DH_\Phi(\omega_M)=0$, where $\omega_M=-\nabla^2\psi_M$ and ψ_M is defined by Eq. (6). We obtain

$$-\Phi''(\omega)=\psi_M'(\omega)=\frac{1}{\sqrt{4\omega^2+(1-\varepsilon^2)^2}} \tag{13}$$

leading to $(1-\varepsilon^2)^{-1}\geqslant-\Phi''(\omega)\geqslant0$. We will need to bound $-\Phi''$ away from zero. Eqs. (5–6) state that

$$\omega=\frac{1-\varepsilon^2}{2}\sinh(4\ \text{Arcth}\ g(x,y))\quad\text{with}$$

$$|g(x,y)|=\left|\frac{\varepsilon\ \cos\ x}{\cosh\ \varepsilon y}\right|\leqslant\varepsilon \tag{14}$$

so that ω is bounded by $|\omega|\leqslant\omega_{\max}\equiv(1-\varepsilon^2/2)\sinh(4\ \text{Arcth}\ \varepsilon)$. The calculation

$$\begin{aligned}\sqrt{4\omega^2+(1-\varepsilon^2)^2}&\leqslant(1-\varepsilon^2)\cosh(4\ \text{Arcth}\ \varepsilon)\\&=\frac{1+6\varepsilon^2+\varepsilon^4}{1-\varepsilon^2}\end{aligned} \tag{15}$$

leads to the improved bounds

$$\frac{-1}{1-\varepsilon^2}\leqslant\Phi''(\omega)\leqslant\frac{-(1-\varepsilon^2)}{1+6\varepsilon^2+\varepsilon^4}. \tag{16}$$

However, the bounds in (16) apply only to $|\omega|\leqslant\omega_{\max}$, whereas we will require such bounds to hold over the entire real line. We therefore construct a function $\tilde{\Phi}$ to coincide with Φ for $|\omega|\leqslant\omega_{\max}$ and with

$$\tilde{\Phi}(\omega)=-\left(\frac{1-\varepsilon^2}{1+6\varepsilon^2+\varepsilon^4}\right)\frac{\omega^2}{2}+\alpha_\pm\omega+\beta_\pm \tag{17}$$

for $|\omega|\geqslant\omega_{\max}$. The constants $\alpha_\pm$ and $\beta_\pm$ are determined by continuity, so that $\tilde{\Phi}$ is a C^2-function.

With these preparations completed, we are ready to define the nonlinear constant of motion:

$$\begin{aligned}\hat{H}_{\tilde{\Phi}}(\delta\omega)&\equiv H_{\tilde{\Phi}}(\omega_M+\delta\omega)-H_{\tilde{\Phi}}(\omega_M)-DH_{\tilde{\Phi}}(\omega_M).\delta\omega\\&=\int\int_D\Big[\frac{1}{2}\delta\omega(-\nabla^2)^{-1}\delta\omega+\tilde{\Phi}(\omega_M+\delta\omega)\\&\qquad-\tilde{\Phi}(\omega_M)-\tilde{\Phi}'(\omega_M).\delta\omega\Big]dx\ dy\end{aligned} \tag{18}$$

and to use it to establish Liapunov stability estimates. Using the bounds (16), we get,

$$\begin{aligned}\left(\frac{1-\varepsilon^2}{1+6\varepsilon^2+\varepsilon^4}\right)\frac{\delta\omega^2}{2}&\leqslant-\tilde{\Phi}(\omega_M+\delta\omega)+\tilde{\Phi}(\omega_M)\\&\quad+\tilde{\Phi}'(\omega_M).\delta\omega\leqslant\frac{1}{1-\varepsilon^2}\frac{\delta\omega^2}{2}.\end{aligned} \tag{19}$$

We introduce $k_{\min}^2$, the minimal eigenvalue of the positive operator $(-\nabla^2)$, to obtain

$$0 \leqslant \int \int_D \frac{1}{2} \delta\omega(-\nabla^2)^{-1} \delta\omega \leqslant \frac{1}{2} k_{\min}^{-2} ||\delta\omega||_{L^2}^2. \tag{20}$$

Combining (19) and (20), we have

$$\left(\frac{1-\varepsilon^2}{1+6\varepsilon^2+\varepsilon^4} - k_{\min}^{-2} \right) ||\delta\omega||_{L^2}^2 \leqslant -2\hat{H}_{\tilde{\Phi}}(\delta\omega)$$

$$\leqslant \frac{1}{1-\epsilon^2} \|\delta\omega\|_{L^2}^2. \tag{21}$$

Now consider an initial value of the perturbation $\delta\omega_0$. Since $\hat{H}_{\tilde{\Phi}}$ is a conserved quantity,

$$-2\hat{H}_{\tilde{\Phi}}(\delta\omega) = -2\hat{H}_{\tilde{\Phi}}(\delta\omega_0) \leqslant \frac{1}{1-\varepsilon^2} ||\delta\omega_0||_{L^2}^2. \tag{22}$$

This *a priori* estimate provides suitable norms bounding the growth of disturbances since we have finally

$$\left[\frac{1-\varepsilon^2}{1+6\varepsilon^2+\varepsilon^4} - k_{\min}^{-2} \right] ||\delta\omega||_{L^2}^2 \leqslant \frac{1}{(1-\varepsilon^2)} ||\delta\omega_0||_{L^2}^2. \tag{23}$$

The solution is nonlinearly stable if the term in brackets is positive.

Consider for the domain D a rectangular box, with length $2\pi N$ in x and 2ℓ in y; the minimal eigenvalue of the operator $(-\nabla^2)$ is $k_{\min}^2 = (1/N^2) + (\pi^2/\ell^2)$, since the eigenfunctions vanishing on the boundary are $f(x,y) = \cos(x/N)\sin(\pi y/\ell)$. Therefore, we have derived a maximum transverse size of the domain D for which the Mallier–Maslowe vortex street is nonlinearly stable. The sufficient conditional stability is the following:

$$\frac{\pi}{\ell} > \sqrt{\frac{1+6\varepsilon^2+\varepsilon^4}{1-\varepsilon^2} - \frac{1}{N^2}}. \tag{24}$$

Figure 2 presents the region of sufficient stability of the counter-rotating vortices in the (ℓ, ε) plane for $N=1$.

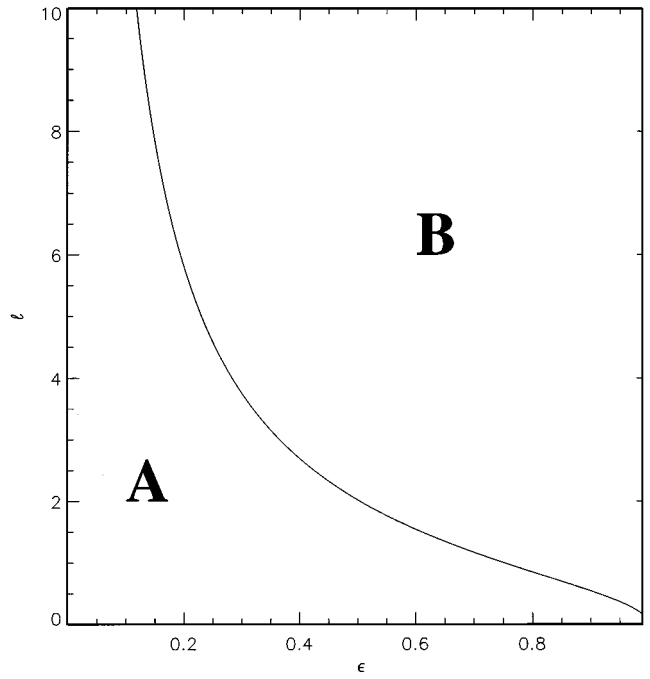

FIG. 2. The region A defines the domain of sufficient stability of a pair of counter-rotating vortices ($N=1$) in the plane (ℓ, ε). ℓ is the transverse size of the box and ε characterizes the vorticity density. The solid line is defined by Eq. (24).

IV. VISCOUS AND FORCED FLOW

A. Introduction

It would be interesting to extend the previously presented results in the presence of viscosity and forcing. Moreover the viscosity imposes a minimum scale $(\nu/\sup\ \omega)^{1/2}$, the diffusion length for the eddy turnover period at the maximum realized vorticity. Thus, a small viscosity avoids some difficulties concerning the continuum limit of Euler flow. To fully understand the nonlinear evolution, we can follow the time evolution of the system from various initial conditions; however, it is useful to obtain the eigenspectrum of the steady states, since they are associated with transitions and loss of stability.

In the viscous case, we have the full two-dimensional Navier–Stokes equation

$$\frac{\partial \nabla^2 \psi}{\partial t} + J(\nabla^2\psi, \psi) = \nu\nabla^4\psi + G_{ext}. \tag{25}$$

In what follows, we will choose the external forcing to counterbalance the viscosity:

$$G_{ext} = -\nu\nabla^4\psi_M \tag{26}$$

for which we shall give a partial justification in Sec. IV D. With the choice (26), if ψ_M is a stationary solution to the Euler equation (3), then ψ_M is also a solution to the full Navier–Stokes equation (25). Viscosity plays an important role, however, in determining the *stability* of the solution ψ_M. Our strategy is to linearize the Navier-Stokes equations around the steady states and to seek eigenmodes of the linearized equations. The linearized equation governing the evolution of a perturbation ϕ is

$$\frac{\partial \nabla^2 \phi}{\partial t} = J(\psi_M, \nabla^2\phi) + J(\phi, \nabla^2\psi_M) + \nu\nabla^4\phi. \tag{27}$$

B. Numerical procedure

All of our calculations are performed on a two-dimensional (x,y) plane. In the periodic x-direction we use a Fourier representation with N_x modes (from 16 to 64); we map $y \in (-\infty, +\infty)$ to $(-1,+1)$ via a tanh mapping with N_y gridpoints (from 65 to 123). Boundary conditions are automatically satisfied in this representation: $\phi(x+2\pi, y) = \phi(x,y)$ and $\partial\phi/\partial y(x, y=\pm\infty) = 0$.

For stability, the viscous term $\nabla^4\phi$ in Eq. (27) is integrated implicitly by the backward Euler scheme. The remaining terms are integrated explicitly. We have

$$\nabla^2\phi_{n+1} = (I - \nu\Delta t\nabla^2)^{-1}[\nabla^2\phi_n + \Delta t(J(\psi_M, \nabla^2\phi_n) + J(\phi_n, \nabla^2\psi_M))]. \tag{28}$$

where Δt is the time step.

The linear stability of ψ_M is determined by the leading eigenvalues (those with greatest real part) of the operator on

the right hand side of (27). The leading eigenvalues of the operator of the differential equation (27) become the dominant ones (those with largest magnitude) of the iterative scheme of Eq. (28); fortunately, dominant eigenvalues are those most readily calculated by iterative methods. Effectively, exact solution of Eq. (27) would require exponentiating the operator on its right hand side, and the numerical method (28) carries out an approximate exponential.

This can be abbreviated as

$$\frac{d\nabla^2\phi}{dt} = A\nabla^2\phi \Leftrightarrow \nabla^2\phi(t) = e^{At}\nabla^2\phi(0) = e^{An\Delta t}\nabla^2\phi(0)$$

$$= B^n\nabla^2\phi(0) \qquad (29)$$

where $t = n\Delta t$ and $B = e^{A\Delta t}$ is approximated by the operator on the right hand side of Eq. (28).

The block power, or Arnoldi's, method is used in order to find the k leading eigenvalues, including complex or multiple eigenvalues, simultaneously, as described by Mamun and Tuckerman[30] and references therein. We first integrate Eq. (27) for some fairly long period of time T in order to purge the vector of the strongly damped eigenmodes which are not important for the linear stability study. We then take k additional time steps, creating $u_1 = u(T), \ldots, u_{k+1} = u(T + kdt)$. The vectors are orthonormalized, forming a basis for what is called the Krylov space. A (k by k) matrix H, which represents the action of B on the Krylov space, is generated and diagonalized, yielding eigenvalues and eigenvectors of the linear stability problem. The eigenvalues λ of A are recovered from those of B (or H) by taking their logarithm and dividing by Δt.

C. Results of the linear stability analysis

Let us now study the linear stability of the Mallier–Maslowe vortices i.e., the stability of the flow ψ_M defined by Eq. (6) with corresponding forcing (26). Figure 3 presents the real part of the two first eigenvalues obtained with the above method as a function of the kinematic viscosity when the vorticity parameter ε is 0.3 in Eq. (5).

In the high viscosity regime ($\nu \gg 1$), the Jacobian terms can be neglected and Eq. (27) becomes

$$\frac{\partial\nabla^2\phi}{\partial t} = \nu\nabla^4\phi \qquad (30)$$

i.e., a heat equation for the vorticity $\nabla^2\phi$ at $\nu \to +\infty$. In this limit, the equation is independent of the vorticity density parameter ε, so the eigenvalues are also independent of ε. The numerical results confirms that, at sufficiently large viscosity and with the forcing chosen according to Eq. (26), the Mallier–Maslowe solutions (6) are stable, since the growth rate of perturbations is negative. Around the value of $\nu = 0.5$, the flow becomes unstable. The growth rate increases as the viscosity decreases. The numerical method presented in Sec. IV B is feasible only for high to moderate viscosities since for low viscosities, stability of the explicit part of the numerical scheme requires a very small time step, leading to a time-consuming code. However, in the zero viscosity limit, we showed in Sec. III that the instability increases with ε.

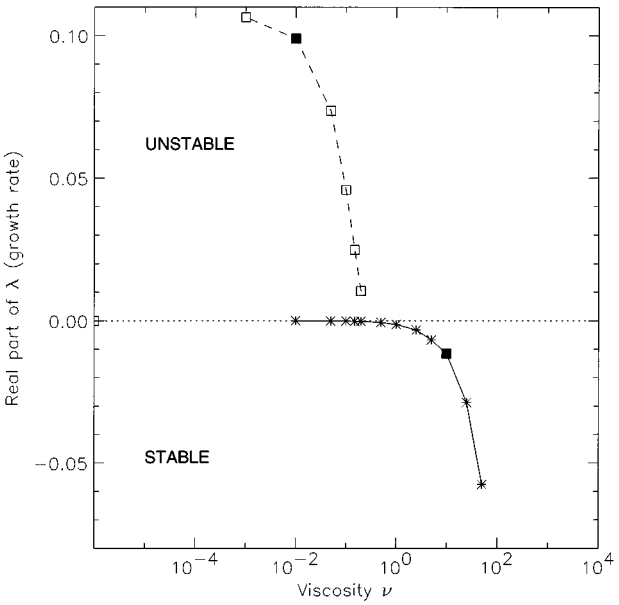

FIG. 3. Eigenvalues. Dependence of the growth rate for the first mode on the viscosity ν for the counter-rotating vortices when $\varepsilon = 0.3$. The squares and the dashed curve correspond to the most unstable (or least stable) eigenvalue and the asterisks and the solid curve to the x-independent mode.

In order to more clearly understand the evolution of the most unstable eigenmodes as a function of the viscosity, we will study the two particular cases depicted by filled squares in Fig. 3, one stable ($\nu = 10$) and the other unstable ($\nu = 0.01$). Figure 4(a) depicts the least stable eigenvector for

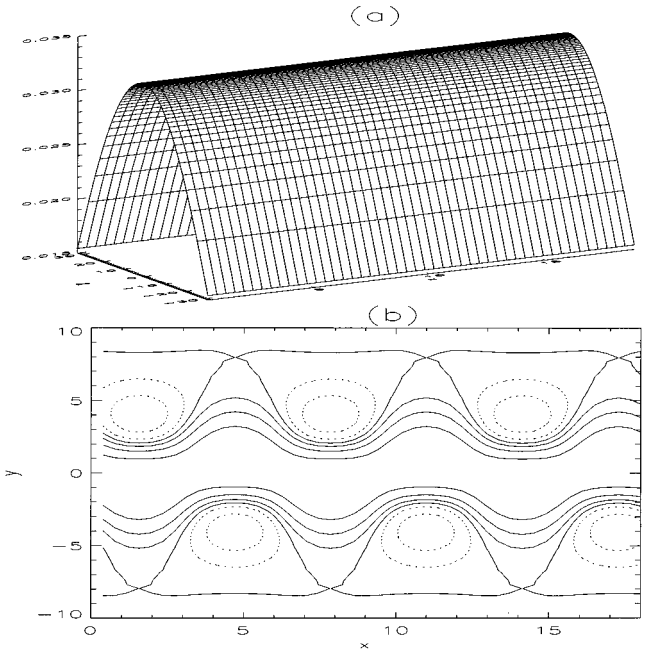

FIG. 4. Eigenvectors. The streamlines of the most unstable eigenvector associated with the Mallier–Maslowe vortices for $\varepsilon = 0.3$ are presented as a surface plot for $\nu = 10$ in (a), while (b) depicts the contour-plot when $\nu = 0.01$. The eigenvalues associated with these eigenvectors are $\lambda = -0.0115$ and $\lambda = 0.099$, respectively.

$\varepsilon=0.3$ and $\nu=10$. As we see, the eigenvector is reflection-symmetric in y and independent of x. This mode resembles a shear layer. The evolution of the eigenvalue shown in Fig. 3 attests that the x-independent mode is not the least unstable mode for low viscosity; however, it is important for the following discussion to notice that this mode is marginally stable for low values of ν. Figure 4(b) presents the contour plot of the most unstable eigenvector for $\varepsilon=0.3$ and $\nu=0.01$. The eigenvector has the shift-and-reflect symmetry $\phi(x+\pi,-y)=\phi(x,y)$ and has the same periodicity in x as ψ_M. The growth rates of the two different modes cross at around the value $\nu=0.5$, as can be seen in Fig. 3.

With the use of a simplified heuristic model it is possible to understand the two modes. Since the flow is mainly present in a confined region, then, for the sake of simplicity, let us consider the main flow to consist of counter-rotating vortices in a finite box: $\psi_0=A\ \sin(kx)\cos(\ell y)$. We approximate the marginally unstable shearing mode by $\phi_1=B\ \cos(\ell y)$, as suggested by Fig. 4(a). With this ansatz, one can then show that the Jacobian term in Eq. (27) will give

$$J(\psi_0,\nabla^2\phi_1)+J(\phi_1,\nabla^2\psi_0)=-\frac{AB\ell k^3}{2}\cos(kx)\sin(2\ell y). \tag{31}$$

The interaction of the basic flow ψ_0 with the marginally unstable mode ϕ_1 thus generates a third term $\phi_2=C\ \cos(kx)\sin(2\ell y)$, completing the triad. We therefore consider an unstable perturbative mode of the form $(\phi_1+\phi_2)$, which will have the same pattern as the most unstable mode found for $\nu=0.01$ and shown in Fig 4(b).

We can go further and explain the occurrence of the instability. We continue to approximate the base flow by $\psi_0=A\ \sin(kx)\cos(\ell y)$, with A fixed, and the perturbation by

$$\phi_1+\phi_2=B(t)\cos(\ell y)+C(t)\cos(kx)\sin(2\ell y). \tag{32}$$

We substitute these approximations into Eq. (27):

$$\frac{\partial\nabla^2(\phi_1+\phi_2)}{\partial t}=J(\psi_0,\nabla^2(\phi_1+\phi_2))+J((\phi_1+\phi_2),\nabla^2\psi_0)+\nu\nabla^4(\phi_1+\phi_2), \tag{33}$$

obtaining

$$\begin{aligned}-\dot{B}\ell^2\ \cos(\ell y)-(k^2+4\ell^2)\dot{C}\ \cos(kx)\sin(2\ell y)&\\ =-\frac{ABk^3\ell}{2}\cos(kx)\sin(2\ell y)-\frac{3}{4}k\ell^3AC[\cos(\ell y)+3\cos(2kx)\cos(\ell y)+3\cos(3\ell y)+\cos(2kx)\cos(3\ell y)]&\\ +\nu(\ell^4B\ \cos(\ell y)+(k^2+4\ell^2)^2C\ \cos(kx)\sin(2\ell y)).&\end{aligned} \tag{34}$$

Projecting onto $\cos(\ell y)$ and $\cos(kx)\sin(2\ell y)$ gives the following Galerkin system for the time dependent amplitudes B and C:

$$\dot{B}=-\nu\ell^2B-\frac{3k}{4}\ell AC, \tag{35a}$$

$$\dot{C}=-\nu(k^2+4\ell^2)C-\frac{k^3\ell}{2(k^2+4\ell^2)}AB. \tag{35b}$$

Finally, looking for solutions $B=B_0e^{st}$ and $C=C_0e^{st}$, one gets the equation

$$s^2+s\nu(k^2+5\ell^2)+\nu^2\ell^2(k^2+4\ell^2)-\frac{3k^4\ell^2A^2}{8(k^2+4\ell^2)}=0. \tag{36}$$

For low values of A (i.e., low value of the intensity of the electric current: see Sec. IV D), the initial flow is stable since all solutions of Eq. (36) are negative. In contrast, above the threshold value

$$A_c=\frac{2\nu(k^2+4\ell^2)}{k^2}\sqrt{\frac{2}{3}}, \tag{37}$$

one solution of Eq. (36) is real and positive: we get a stationary bifurcation giving rise to an instability of the perturbation $(\phi_1+\phi_2)$ whose pattern coincides with that shown in Fig. 4(b). This simple approach therefore gives a good qualitative understanding of the relationship between the marginal and unstable modes, and of the onset of instability.

Figure 5 shows the evolution of the greatest eigenvalue versus viscosity for three different values of ε on a logarithmic scale. We see that the results are independent of ε in the diffusive regime (high viscosity), as explained in the preceding section. The inset allows us to ascertain that the value of λ is a linear decreasing function of the viscosity. In the low viscosity regime the evolution is qualitatively the same but the curves are distinct. The bigger the parameter ε, the bigger the leading eigenvalue and, therefore the more unstable the flow. One can also verify that the Mallier–Maslowe vortices with $\varepsilon=0.5$ become unstable at a critical viscosity ν_c which is slightly higher than that corresponding to $\varepsilon=0.2$: the critical viscosity ν_c is an increasing function of ε.

D. Relation to the experiment

In the experiment by Tabeling *et al.*,[9] the typical velocity V of the basic regime can be found by balancing the forcing with the viscous term, as we have done via our assumption (26). In dimensional terms, this leads to the relation

$$V=\frac{BhI}{\ell\nu\rho} \tag{38}$$

in which B is the maximum value of the magnetic field, I the intensity of the electric current, h the depth of the fluid layer,

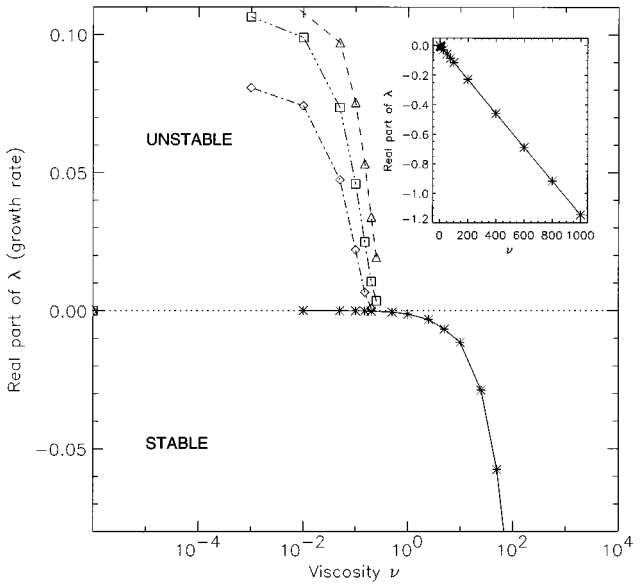

FIG. 5. Dependence of the growth rate on viscosity for three values of ε for the counter-rotating vortices. The diamonds and the dash-dotted curve correspond to $\varepsilon=0.2$, the squares and the dash-triple-dotted curve correspond to $\varepsilon=0.3$ and the triangles and the dashed curve correspond to $\varepsilon=0.5$. The asterisks and the solid curve represent the x-independent mode. A logarithmic scale is used for the viscosity; the inset uses a linear scale.

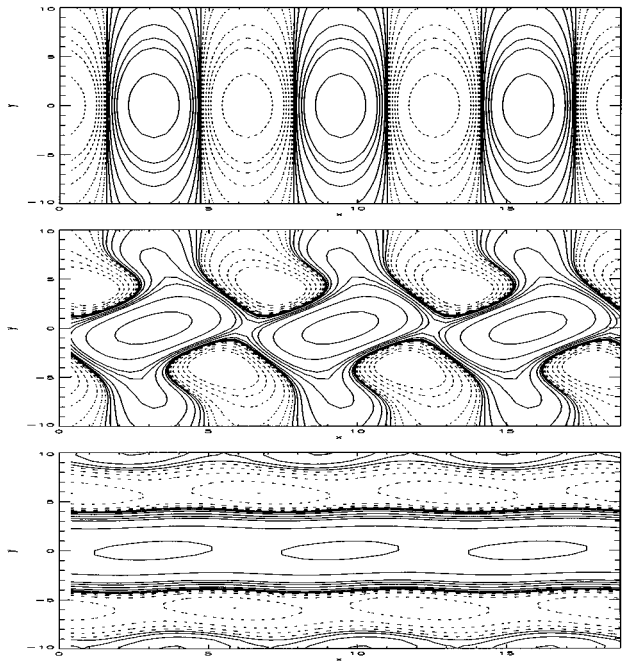

FIG. 6. Contour plot of the stream function for $\varepsilon=0.3$ and $\nu=0.01$. (a) initial condition, the Mallier–Maslowe ψ_M; (b) $t=65$; (c) $t=200$.

ℓ the width of the magnet, ν the viscosity and ρ the density of the fluid. Because the typical velocity varies linearly with I, it is reasonable to suppose that the streamfunction and its derivatives will also increase linearly with I. We thus take our streamfunction $\psi=\xi\psi_M$, where ψ_M is the Mallier–Maslowe solution (9) and ξ is a scalar which increases with I.

One can easily check that if ψ_e is any solution to the stationary solution Euler equation (2), then $\xi\psi_e$ is also a solution. Let us show that the linear stability of all the solutions $\xi\psi_e$ is determined by a linear stability analysis of ψ_e as a function of viscosity. The equation governing the evolution of an infinitesimal perturbation ϕ to the new inviscid solution is

$$\frac{\partial\nabla^2\phi}{\partial t}=J(\xi\psi_e,\nabla^2\phi)+J(\phi,\nabla^2\xi\psi_e)+\nu\nabla^4\phi. \tag{39}$$

Dividing by ξ, we get

$$\frac{1}{\xi}\frac{\partial\nabla^2\phi}{\partial t}=J(\psi_e,\nabla^2\phi)+J(\phi,\nabla^2\psi_e)+\frac{\nu}{\xi}\nabla^4\phi. \tag{40}$$

Thus, studying the linear stability of the solution $\xi\psi_e$ for viscosity ν is equivalent to studying the linear stability of the solution ψ_e for viscosity (ν/ξ), except that the eigenvalue will also be modified by ξ.

Using this insight, it is then possible to understand the appearance of the instability. Recall from Fig. 3 that the counter-rotating vortex flow ψ_M is stable for sufficiently high ν. Thus $\xi\psi_M$ is stable for sufficiently high ν/ξ, i.e., for sufficiently low electric current. Increasing the electric current I in the experiment corresponds to increasing ξ and, therefore, to decreasing the ''renormalized'' viscosity (ν/ξ). The solution will therefore remain stable until the renormalized viscosity reaches the critical viscosity ν_c shown in Fig. 3. Above this threshold, the counter-rotating vortices will be unstable and will evolve as presented in the next section. The appearance of the instability of the counter-rotating vortices for a high enough electric current I is thus explained.

V. TIME INTEGRATION AND CONCLUSION

The transitions resulting from the linear instability of the Mallier–Maslowe vortices are studied by time-integrating the Navier–Stokes equation (25). This numerical experiment is constructed to resemble that of Tabeling *et al.*, except that the size of the box is infinite. As an initial condition, we add to the Mallier–Maslowe vortex flow ψ_M a small perturbation of the form $\phi(x,y,t=0)=\exp(-y^2)\cos x$, to accelerate the appearance of the possible unstable modes. The spatial representation is, as discussed in Sec. IV B, with a resolution of $N_x=32$, $N_y=69$ and $y_{\max}=15$. The time stepping is carried out according to Eq. (28), with $\Delta t=0.01$.

If the simulation is carried out with $\varepsilon=0.3$ and $\nu=5$, the patterns are stable, confirming the linear stability analysis presented in the previous section. When the parameters ε and ν are fixed at 0.3 and 0.01 respectively, the evolution, depicted in Fig. 6, is clearly different. We see in Fig. 6(b) that at $t=65$ we have a linear array of tilted vortices of positive sign and the size of the vortices has doubled as occurred in the experiment. The negative vortices have been ejected away from the center of the box.

If we plot the deviation $\phi=(\psi-\psi_M)$ from the initial condition ψ_M, we find in the initial stage (at $t=50$ for example) the stream function presented in Fig. 7(a), confirming

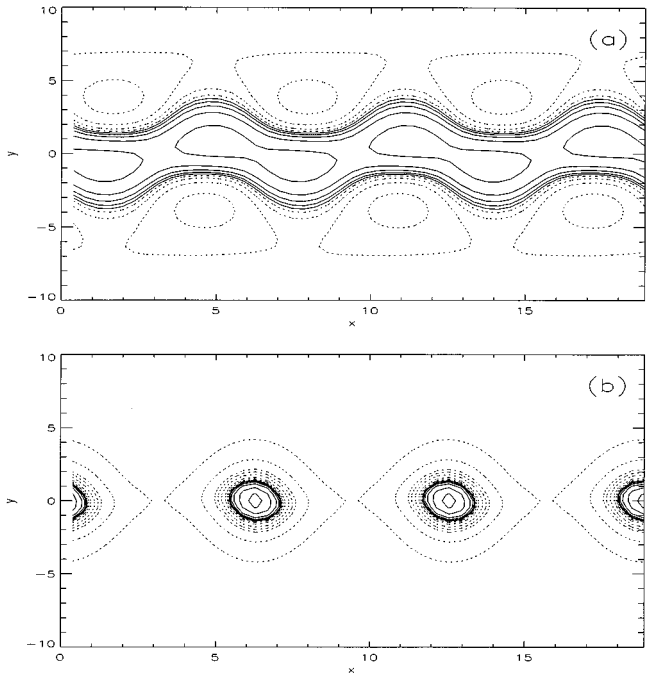

FIG. 7. Contour plot of the deviation $\phi=\psi-\psi_M$ from the Mallier–Maslowe solution for $\varepsilon=0.3$, $\nu=0.01$ and $\mu=0$. (a) $t=50$; (b) $t=3000$.

the linear stability analysis [see Fig. 4(b)]. After this linear transient growth, the flow continues to evolve until it approaches the pattern depicted in Fig. 6(c). However, the amplitude continues to increase with time (see Fig. 8), while preserving the pattern. Figure 7(b) depicts the deviation ϕ at $t=200$ and we note that the pattern around the x-axis resembles somewhat the Kelvin–Stuart vortices [see Fig. 1(b)].

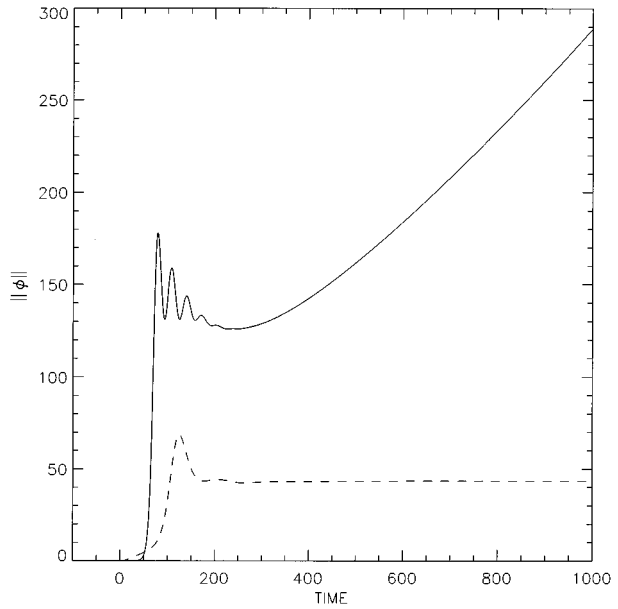

FIG. 8. Evolution of the norm of the deviation $||\phi||=||\psi-\psi_M||$ from the Mallier–Maslowe solution for $\varepsilon=0.3$, $\nu=0.01$ versus time. The solid curve corresponds to $\mu=0$ and the dashed curve to $\mu=0.01$.

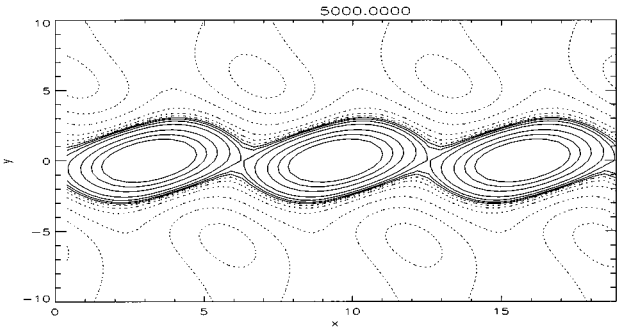

FIG. 9. Contour plot of the stream function ψ for $\varepsilon=0.3$, $\nu=0.01$ and $\mu=0.01$ at $t=5000$.

This explains why the system does not reach a final equilibrium state: Since ϕ is then itself a solution of the stationary inviscid Eq. (3) $J(\phi,\nabla^2\phi)=0$, the nonlinear saturation effect disappears and ϕ continues to grow in time. A similar case was found in zero Prandtl number convection, where the linearly unstable roll modes are exact nonlinear solutions.[31]

One possible reason that our simulation, unlike the experiment of Tabeling *et al.*,[9] does not reach a final equilibrium state could be that we considered the flow to be perfectly two-dimensional. In the experiment, two-dimensionality is enforced by using a shallow fluid layer: a frictional force proportional to the velocity could capture this bottom-friction effect.[32,33] The addition of a term $-\mu\nabla^2\psi$ proportional to the velocity on the right hand side of Eq. (25) will change the evolution of the flow. The eigenvalues in the presence of linear friction differ from those of the problem without friction only by a shift $(-\mu)$ of the growth rate: thus the determination of the dependence of the eigenvalue spectrum on μ does not require additional numerical studies and, in addition, the linear friction is always stabilizing.

We therefore time-integrate this system, including the linear friction term as well as the ordinary viscosity. The external force is now chosen as

$$G_{ext}=-\nu\nabla^4\psi_M+\mu\nabla^2\psi_M \tag{41}$$

so that, as in the previous section, the viscosity only acts on the perturbation not the basic flow. The resulting streamfunction at $t=300$ is shown in Fig. 9 for a small value of μ fixed at 0.01. Contrary to the case without linear friction ($\mu=0$, see Fig. 6), the flow attains an equilibrium state with co-rotating vortices along the x-axis as demonstrated by the time series in Fig. 8. Thus, the linear friction term stabilizes the row of co-rotating vortices as was obtained in the experiment. The necessity of this linear friction term in reproducing the final state of the experiment could be a reason why the final maximum entropy state is not often reached by Marteau *et al.*[20] in their experiment: in their small 2D lattice of electromagnetically forced vortices, the bottom-friction effect should also be important.

The purpose of this work was to understand and explain the behavior of the instructive experiment of Tabeling *et al.*[9] First, we derived explicitly the nonlinear stability condition

for the counter-rotating vortex solutions in a rectangular box without compensating viscosity; the finite-size effects of the box were studied. Then, introducing viscosity and compensating forcing, we derived a model for the appearance of the instability when the electric current is increased: the renormalized viscosity decreases until it reaches the critical viscosity ν_c determined by a numerical linear stability analysis. We found ν_c to be an increasing function of the parameter ε characterizing the vorticity which could explain the fact low vorticity-flows [i.e., low ε in Eq. (5)] are more visible in 2D hydrodynamic flows, since they are more stable than high vorticity-flows. Above this threshold, the evolution of the system leads to a final equilibrium state similar to that in the experiment if a linear term is added to the standard Navier–Stokes equation to reproduce the effects of the friction at the bottom of the experimental apparatus.

ACKNOWLEDGMENTS

The authors thank D. D. Holm, A.C. Newell and S. Takeno for helpful discussions.

[1]P. G. Saffman, *Vortex Dynamics* (Cambridge University Press, Cambridge, 1992).
[2]G. R. Flierl, ''Isolated eddy models in geophysics,'' Annu. Rev. Fluid Mech. **19**, 493 (1987).
[3]Y. Couder and C. Basdevant, ''Experimental and numerical study of vortex couples in two-dimensional flows,'' J. Fluid. Mech. **173**, 225 (1986).
[4]R. T. Pierrehumbert and S. E. Widnall, ''The structure of organized vortices in a free shear layer,'' J. Fluid Mech. **102**, 301 (1981).
[5]G. J. F. van Heijst and R. C. Kloosterziel, ''Dipole formation and collisions in a stratified fluid,'' Nature **340**, 212 (1989).
[6]E. J. Hopfinger and G. J. F van Heijst, ''Vortices in rotating fluids,'' Annu. Rev. Fluid Mech. **25**, 241 (1993).
[7]J.-M. Nguyen Duc and J. Sommeria, ''Experimental characterization of steady two-dimensional vortex couples,'' J. Fluid Mech. **192**, 175 (1988).
[8]N. F. Bondarenko and M. Z. Gak, ''Application of magnetohydrodynamic effects in Electrolytes to model rotational hydrodynamic processes,'' Bull. (Izv.) Acad. Sci. USSR, Atmos. Ocean. Phys. **14**, 207 (1978).
[9]P. Tabeling, B. Perrin and S. Fauve, ''Instability of a linear array of forced vortices,'' Europhys. Lett. **3**, 459 (1987).
[10]O. Cardoso, D. Marteau, and P. Tabeling, ''Quantitative experimental study of the free decay quasi-two-dimensional turbulence,'' Phys. Rev. E **49**, 454 (1994), and references therein.
[11]G. M. Zaslavsky *et al.*, *Weak Chaos and Quasi Regular Patterns* (Cambridge Nonlinear Science Series, 1991).
[12]H. Lamb, *Hydrodynamics* (Cambridge University Press, Cambridge, 1932).
[13]J. J. Rasmussen *et al.*, ''Dipolar vortices in two-dimensional flows,'' in *Nonlinear Dynamical Phenomena in Physical, Chemical and Biological Systems*, edited by Christiansen and Mosekilde (IMACS, Lingby, 1994), p. 1.
[14]V. V. Meleshko and G. J. F. van Heijst, ''On Chaplygin's investigations of two-dimensional vortex structures in an inviscid fluid,'' J. Fluid Mech. **272**, 157 (1994).
[15]A. C. Ting, H. H. Chen, and Y. C. Lee, ''Exact vortex solutions of two-dimensional guiding-center plasmas,'' Phys. Rev. Lett. **53**, 1348 (1984).
[16]A. C. Ting, H. H. Chen, and Y. C. Lee, ''Exact solutions of a nonlinear boundary value problem: the vortices of the two dimensional sinh-Poisson equation,'' Physica D **26**, 37 (1987).
[17]R. A. Pasmanter, ''On long lived vortices in 2D viscous flows, most probable states of inviscid flows and a soliton equation,'' Phys. Fluids **6**, 1236 (1994).
[18]G. Joyce and D. Montgomery, ''Statistical mechanics of negative temperature states,'' Phys. Fluids **17**, 1139 (1973).
[19]J. Sommeria, C. Staquet, and R. Robert, ''Final equilibrium state of a two-dimensional shear layer,'' J. Fluid Mech. **233**, 661 (1991).
[20]D. Marteau, O. Cardoso, and P. Tabeling, ''Equilibrium states of 2D turbulence: an experimental study,'' Phys. Rev. E **51**, 5124 (1995).
[21]R. Mallier and S. A. Maslowe, ''A row of counter-rotating vortices,'' Phys. Fluids A **5**, 1074 (1993).
[22]J. T. Stuart, ''On finite amplitude oscillations in laminar mixing layers,'' J. Fluid Mech. **29**, 417 (1967).
[23]J. Liouville, ''Sur l'équation aux différences partielles $(\partial^2 \ln \lambda/\partial u \partial v) \pm (\lambda/2a^2) = 0$,'' J. Math. **18**, 71 (1853).
[24]H. Poincaré, ''Les fonctions fuchsiennes et l'équation $\Delta u = e^u$,'' J. Math. **4**, 137 (1898).
[25]J. L. Gervais and A. Neveu, ''The dual string spectrum in Polyakov quantization (I),'' Nucl. Phys. B **199**, 59 (1982).
[26]E. R. Tracy, C. H. Chin, and H.H. Chen, ''Real periodic solutions of the Liouville Equation,'' Physica D **23**, 91 (1986).
[27]D. D. Holm, J. E. Marsden, and T. Ratiu, ''Nonlinear stability of the Kelvin-Stuart cat's eyes flow,'' AMS Lectures Appl. Math. **23**, 171 (1986).
[28]T. Dauxois, ''Nonlinear stability of counter-rotating vortices,'' Phys. Fluids **6**, 1625 (1994).
[29]D. D. Holm, J. E. Marsden, T. Ratiu, and A. Weinstein, ''Nonlinear stability of fluid and plasma equilibria,'' Phys. Rep. **123**, 1 (1985).
[30]C. K. Mamun and L. S. Tuckerman, ''Asymmetry and Hopf bifurcation in spherical Couette flow,'' Phys. Fluids **7**, 80 (1995).
[31]K. Kumar, S. Fauve, and O. Thual, ''Zero Prandtl number convection'' (submitted).
[32]K. Gotoh, Y. Murakani, and N. Matsuda, ''Large-scale and periodic modes of rectangular cell flow,'' Phys. Fluids **7**, 302 (1995).
[33]A. Thess, ''Instabilities in two-dimensional spatially periodic flows. Part I: Kolmogorov flow,'' Phys. Fluids A **4**, 1385 (1992).